



Supplement of

DynQual v1.0: a high-resolution global surface water quality model

Edward R. Jones et al.

Correspondence to: Edward R. Jones (e.r.jones@uu.nl)

The copyright of individual parts of the supplement might differ from the article licence.

S1. Pollutant loadings

Pollutant loadings can be either be: 1) prescribed by the user directly; or 2) calculated within the DynQual run by providing simple input data. When loadings are prescribed directly to the model, the user is only required to provide input files on the total (i.e. combined) pollutant loadings of TDS (in g day⁻¹), BOD (in g day⁻¹), FC (in 10⁶ cfu day⁻¹) and Tw (in MW). Conversely, when pollutant loadings are calculated within DynQual, a variety of input data is required to reflect both pollutant emissions from sectoral activities and the transmission of pollution to the environment (Jones et al., 2022). Loadings calculated using DynQual are in consistent units across all sectors: g day⁻¹ for TDS and BOD and 10⁶ cfu day⁻¹ for FC. The subsequent routing of pollutants through the stream network and the calculation of in-stream concentrations follows the same approach in both configurations.

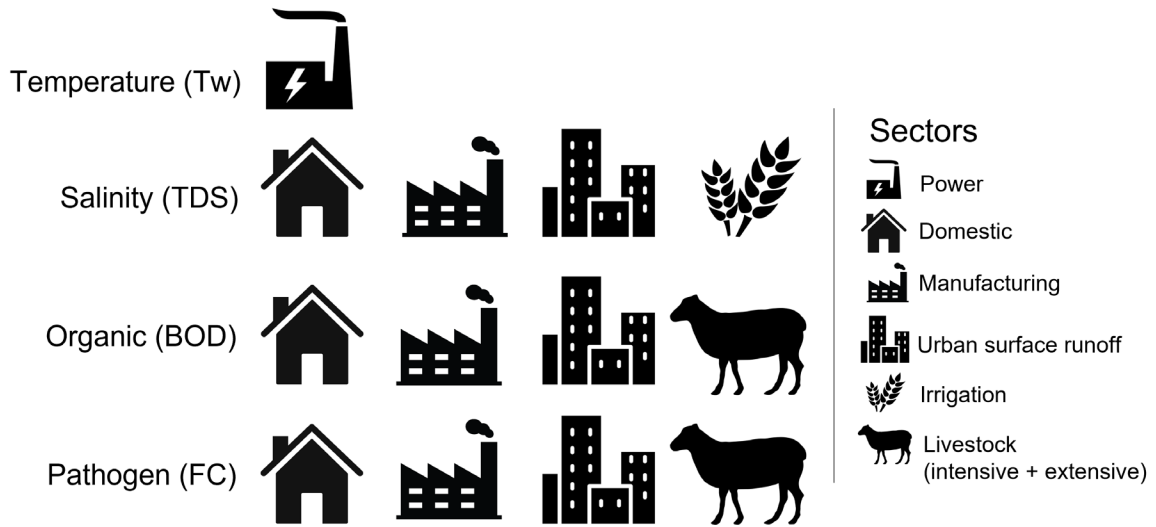


Figure S1. Simplified approach for pollutant routing and the calculation of in-stream concentrations.

The following section describes the approach used and assumptions made for calculating pollutant loadings dynamically within a DynQual model run. DynQual considers pollutant emissions from five distinct sectors (domestic, manufacturing, livestock, irrigation and thermo-electric power generation) and from urban surface runoff (Figure S1). The prevalence of wastewater collection and treatment, combined with their associated pollutant removal efficiencies, are key factors controlling subsequent delivery of pollution to surface waters (Jones et al., 2022). The fraction of pollutant loadings removed by wastewater treatment (-) are estimated for the domestic ($R_{dom,p,n}$), manufacturing ($R_{man,p,n}$) and intensive livestock ($R_{intLiv,p,n}$) sectors, and from urban surface runoff ($R_{USR,p,n}$) by multiplying the fraction of each treatment level occurring in a gridcell by the pollutant removal efficiency associated with that treatment level [S1].

$$R_{dom,p,n} = (f_{ter_n} \cdot r_{ter_p} + f_{sec_n} \cdot r_{sec_p} + f_{pri_n} \cdot r_{pri_p}) + (f_{bs_n} \cdot r_{bs_p}) + (f_{od_n} \cdot (1 - s_n))$$

$$R_{man,p,n} = f_{ter_n} \cdot r_{ter_p} + f_{sec_n} \cdot r_{sec_p} + f_{pri_n} \cdot r_{pri_p}$$

$$R_{USR,p,n} = f_{ter_n} \cdot r_{ter_p} + f_{sec_n} \cdot r_{sec_p} + f_{pri_n} \cdot r_{pri_p}$$

$$R_{intLiv,p,n} = (f_{ter_n} + f_{sec_n}) \cdot r_{sec_p}$$

[S1]

Where: f is the fraction of tertiary+ treatment (f_{ter_n}), secondary treatment (f_{sec_n}) and primary treatment (f_{pri_n}) within gridcell n , and r is the removal efficiency associated with tertiary ($r_{ter_p,r}$),

30 secondary ($r_{sec,p,r}$) and primary ($r_{pri,p,r}$) treatment per pollutant p . f_{bs_n} and f_{od_n} is the fraction of basic
 sanitation and open defecation, respectively, within gridcell n . r_{bs_i} is the reduction in pollutant p from
 basic sanitation collection facilities and s_n is the gridcell specific surface runoff fraction. For more
 detailed information about the development and implementation of gridcell specific wastewater
 treatment practices and their inclusion in DynQual, we refer to previous work (Jones et al., 2021;
 35 Jones et al., 2022).

S1.1 Domestic

$$L_{dom,p,n} = Pop_n \cdot E_{dom,p,n} \cdot (1 - R_{dom,p,n})$$

40 [S2]

Pollutant loadings from the domestic sector ($L_{dom,p,n}$) are calculated by multiplying the total
 population (Pop_n) in gridcell n by a regional-specific per capita excretion rate ($E_{dom,p,n}$) of pollutant
 p (TDS and BOD in $g\ capita^{-1}\ day^{-1}$; FC in $cfu\ capita^{-1}\ day^{-1}$) [S2]. Pollutant loadings are abated based
 upon gridcell specific domestic wastewater collection and treatment practices, represented by
 45 $R_{dom,p,n}$ (-), which depends upon the wastewater pathway(s) in gridcell n and the pathway-specific
 removal efficiency of pollutant p (Jones et al., 2021; Jones et al., 2022).

Gridded population data at 5 arc-minutes and annual temporal resolution was obtained from ISIMIP3a
 (Lange and Geiger, 2020). Per capita pollutant loadings are prescribed per water quality constituent at
 the regional scale (Table S1). Per capita excretion rates of BOD and FC vary at the regional level due
 50 to differences in diet, climate and health status (Williams et al., 2012; UNEP, 2016). Conversely, due
 to a lack of more detailed data, an average global value for per capita excretion of TDS was used.
 Pollutant loadings per capita are based on extensive literature research conducted for previous global
 water quality modelling studies (UNEP, 2016; Van Vliet et al., 2021) and are assumed to remain
 constant throughout the study period.

55 **Table S1.** Per capita excretion rates of total dissolved solids (TDS), biological oxygen demand (BOD)
 and fecal coliform (FC) loadings per geographic region.

Geographic Region	Domestic		
	TDS ($g\ day^{-1}\ capita^{-1}$)*	BOD ($g\ day^{-1}\ capita^{-1}$)**	FC ($cfu\ day^{-1}\ capita^{-1}$ ***)
North America	100	65	$1.3 \cdot 10^{10}$
Latin America & Caribbean	100	56	$1.4 \cdot 10^{10}$
Western Europe	100	60	$1.3 \cdot 10^{10}$
Middle East & North Africa	100	45	$1.8 \cdot 10^{10}$
Sub-Saharan Africa	100	37	$4.7 \cdot 10^9$
Southern Asia	100	40	$1.9 \cdot 10^{10}$
Eastern Europe & Central Asia	100	50	$1.6 \cdot 10^{10}$
East Asia & Pacific	100	50	$1.6 \cdot 10^{10}$

60 *as per UNEP (2016) and van Vliet et al. (2021); **as per UNEP (2016) and Williams et al., (2012); ***as per
 UNEP (2016) and Reder et al., (2015)

S1.2 Manufacturing

$$L_{man,p,n} = WW_{man,n} \cdot C_{man,p,n} \cdot (1 - R_{man,p,n})$$

65

[S3]

Pollutant loadings from the manufacturing sector ($L_{man,p,n}$) are calculated by multiplying the manufacturing wastewater flows (return flows) in gridcell n ($WW_{man,n}$ in $\text{m}^3 \text{ day}^{-1}$) by a mean manufacturing effluent concentration ($C_{man,p,n}$) for pollutant p (TDS and BOD in mg l^{-1} ; FC in $\text{cfu } 100\text{ml}^{-1}$) [S3]. Pollutant loadings are abated based upon gridcell-specific manufacturing wastewater collection and treatment practices, represented by $R_{man,p,n}$ (-) which depends upon the wastewater pathway(s) in gridcell n and the pathway-specific removal efficiency of pollutant p (Jones et al., 2021; Jones et al., 2022).

As PCR-GLOBWB2 does not distinguish explicitly between the manufacturing and thermoelectric power sectors (lumped together as the “industrial” sector), we estimate the percentage of total industrial flows that originate specifically from manufacturing activities and apply this to PCR-GLOBWB2 simulated industrial return flows at the country level. To make this distinction, we subtract power return flows derived from an external source (Lohrmann et al., 2019) from PCR-GLOBWB2 industrial return flows, to provide an estimate of manufacturing return flows. We further cross-checked these estimated manufacturing return flows against a spatially-explicit municipal wastewater dataset (Jones et al., 2021).

Lacking more detailed information regarding both the specific manufacturing processes and the associated effluent quality, globally consistent effluent concentrations are applied for all manufacturing return flows worldwide (Table S2), consistent with previous work (UNEP, 2016; Van Vliet et al., 2021). Mean effluent concentrations are derived from literature review and are assumed to remain constant throughout the study period.

Table S2. Effluent concentrations of total dissolved solids (TDS), biological oxygen demand (BOD) and fecal coliform (FC) from the manufacturing sector.

	TDS (mg l^{-1})*	BOD (mg l^{-1})*	FC ($\text{cfu } 100\text{ml}^{-1}$)*
Global	3000	400	$3.55 \cdot 10^6$

*as per UNEP (2016) and van Vliet et al. (2021)

90

S1.3 Urban surface runoff

$$L_{USR,p,n} = RF_{USR,n} \cdot C_{USR,p,n} \cdot (1 - R_{USR,p,n})$$

95

[S4]

Pollutant loadings from urban surface runoff ($L_{USR,p,n}$) are calculated by multiplying daily urban surface return flows ($RF_{USR,n}$ in $\text{m}^3 \text{ day}^{-1}$) in gridcell n by a mean urban runoff effluent concentration ($C_{USR,p,n}$) for pollutant p (TDS and BOD in mg l^{-1} ; FC in $\text{cfu } 100\text{ml}^{-1}$) [S4]. Pollutant loadings are abated based upon gridcell-specific wastewater collection and treatment practices, represented by $R_{USR,p,n}$ (-) which depends upon the wastewater pathway(s) in gridcell n and the pathway-specific removal efficiency of pollutant p (Jones et al., 2021; Jones et al., 2022).

100

Urban surface runoff flows are simulated within PCR-GLOBWB2 (Sutanudjaja et al., 2018), calculated by multiplying the fraction of the gridcell that is urban by the simulated surface runoff. Mean urban surface runoff pollutant concentrations are taken from existing work (UNEP, 2016), based on extensive literature review. TDS and BOD concentrations vary at the regional level whereas, lacking detailed data, FC is assumed to be constant across all regions (Table S3). Mean urban surface runoff concentrations are assumed to remain constant throughout the study period.

Table S3. Urban surface runoff total dissolved solids (TDS), biological oxygen demand (BOD) and fecal coliform (FC) mean concentrations per geographic region.

Region	Urban surface runoff		
	TDS (mg l ⁻¹)*	BOD (mg l ⁻¹)*	FC (cfu 100ml ⁻¹)*
North America	205	12	1·10 ⁶
Latin America & Caribbean	205	12	1·10 ⁶
Western Europe	205	12	1·10 ⁶
Middle East & North Africa	212	19	1·10 ⁶
Sub-Saharan Africa	178	62	1·10 ⁶
Southern Asia	246	105	1·10 ⁶
Eastern Europe & Central Asia	246	19	1·10 ⁶
East Asia & Pacific	246	105	1·10 ⁶

*as per UNEP (2016)

S1.4 Livestock

For calculating pollutant loadings from the livestock sector, the sector is sub-divided into intensive and extensive systems based on livestock population density. For defining intensive livestock systems, a minimum threshold density of 25 livestock units per km² was set with one livestock unit equivalent to ~250kg (1 bovine) (Wen et al., 2017; Vigiak et al., 2019). Average animal mass equivalent coefficients were taken from literature (Robinson et al., 2011; Wen et al., 2017) to convert this threshold density into a livestock-type specific threshold density per km² (Table S4) (Wen et al., 2017; Vigiak et al., 2019). Gridcells exceeding this threshold density (per livestock type) were designated as intensive livestock systems, whereas gridcells below this threshold were designated as extensive livestock systems.

The distinction between intensive and extensive livestock systems is made to account for the differences in the paths by which livestock waste (manure) enters the stream network, namely whether there is transportation by surface runoff (for extensive systems) or whether there is collection (and potentially subsequent treatment) of livestock waste (for intensive systems). Abatement of collected livestock waste is all assumed to be at the same level as secondary treatment in line with Wen et al (2017) and occurs only in gridcells where municipal wastewater treatment is also occurring. The waste is subsequently assumed to be spread to land as manure and transported to surface waters via surface runoff. This approach for calculating pollutant loadings from the livestock sector is line with previous work (Wen et al., 2017; Vigiak et al., 2019).

Table S4. Threshold density for designation of livestock activities as intensive systems, per livestock type.

Livestock type	Animal mass equivalent coefficient*	Threshold density (stock km ⁻²)
Buffalo	1	25
Chicken	0.01	2500
Cow	1	25
Duck	0.01	2500
Goat	0.1	250
Horse	1	25
Pig	0.3	83
Sheep	0.1	250

* as per Robinson et al. (2011) and Wen et al. (2017)

140

Pollutant loadings from the livestock sector are calculated as per Eq. [S5], in line with the previous approaches for calculating pollutant loadings from intensive (Wen et al., 2017; Vigiak et al., 2019) and extensive (Van Vliet et al., 2021) livestock systems:

145

$$L_{intLiv,p,n} = \sum_y (LivPop_{y,n} * E_{liv,y,p,n}) \cdot (1 - R_{intLiv,p,n}) \cdot s_n$$

$$L_{extLiv,p,n} = \sum_y (LivPop_{y,n} \cdot E_{liv,y,p,n}) \cdot s_n$$

[S5]

150

Where: $L_{intLiv,p,n}$ and $L_{extLiv,p,n}$ represent the loadings of pollutant p in gridcell n from the intensive and extensive livestock sectors, respectively. $LivPop_{y,n}$ is the total livestock population in gridcell n per livestock type y , with 8 separate livestock types considered (buffalo, chicken, cow, duck, goat, horse, pig, sheep). $E_{liv,y,p,n}$ is the per stock excretion rate of pollutant p (BOD in g stock⁻¹ day⁻¹; FC in cfu stock⁻¹ day⁻¹) of livestock type y and gridcell n . s_n is the fraction surface runoff in gridcell n and $R_{intLiv,p,n}$ is the removal fraction of pollutant p due to livestock waste management practices in gridcell n (Jones et al., 2021; Jones et al., 2022).

155

160

Gridded livestock numbers at 5 arc-minutes are derived at the annual timescale from a global dataset for the reference year of 2010 (Gilbert et al., 2018). Thus, we do not account for intra-annual variations in livestock numbers. For the quantification of past gridded livestock numbers, a region-specific (annual) constant percentage change in the number of animals per livestock type is applied to all gridcells based on data from the FAO (Thomson, 2003) (Table S5).

Table S5. Annual growth in livestock type (population number) between 1999 – 2030 (%), applied to gridded livestock populations for 1980 – 2019 (Thomson, 2003)

Region	Livestock Type (% annual change)				
	Cattle & Buffalo	Sheep & Goats	Pigs	Horses	Chickens & Ducks
North America	-0.1	0.2	0.1	0	0.6
Latin America & Caribbean	1	0.6	1.1	0	1.9
Western Europe	-0.1	0.2	0.1	0	0.6
Middle East & North Africa	1.5	1	0	0	2.1
Sub-Saharan Africa	1.1	1.2	1.4	0	2.2
Southern Asia	0.3	1.1	1	0	3.6
Eastern Europe & Central Asia	1.2	1.2	0.8	0	1.5
East Asia & Pacific	1.2	1.2	0.8	0	1.5

Excretion rates of BOD (Table S6) and FC (Table S7) per livestock type y and per region were determined through literature study, as per previous global water quality modelling studies (UNEP, 2016; Van Vliet et al., 2021). Excretion rates of pollutants per livestock type is assumed constant throughout the study period.

Table S6. Biological oxygen demand (BOD) loadings per animal per livestock type and geographic region.

Region	Biological Oxygen Demand ($\text{g day}^{-1} \text{stock}^{-1}$)*							
	Buffalo	Chicken	Cow	Duck	Goat	Horse	Pig	Sheep
Western Europe	400	8.3	400	8.3	50	300	233	50
Sub-Saharan Africa	240	8.3	240	8.3	50	300	186.4	35
Southern Asia	200	8.3	200	8.3	50	300	233	35
North America	400	8.3	400	8.3	50	300	233	50
Middle East & North Africa	280	8.3	280	8.3	50	300	186.4	35
Latin America & Caribbean	280	8.3	280	8.3	50	300	233	35
Eastern Europe & Central Asia	240	8.3	240	8.3	50	300	233	35
East Asia & Pacific	280	8.3	280	8.3	50	300	233	35

* as per Robinson et al., (2011), Wen et al., (2017), Vigiak et al., (2019), van Vliet et al., (2021).

Table S7. Fecal coliform (FC) loadings per animal per livestock type and geographic region.

Region	Fecal coliform (cfu day ⁻¹ stock ⁻¹)*							
	Buffalo	Chicken	Cow	Duck	Goat	Horse	Pig	Sheep
Western Europe	1.01·10 ¹¹	1.36·10 ⁸	1.01·10 ¹¹	2.43·10 ⁹	1.20·10 ⁹	1.40·10 ⁹	1.08·10 ¹⁰	1.12·10 ⁹
Sub-Saharan Africa	6.06·10 ¹⁰	1.36·10 ⁸	6.06·10 ¹⁰	2.43·10 ⁹	1.20·10 ⁹	1.40·10 ⁹	8.64·10 ⁹	7.84·10 ⁸
Southern Asia	5.05·10 ¹⁰	1.36·10 ⁸	5.05·10 ¹⁰	2.43·10 ⁹	1.20·10 ⁹	1.40·10 ⁹	1.08·10 ¹⁰	7.84·10 ⁸
North America	1.01·10 ¹¹	1.36·10 ⁸	1.01·10 ¹¹	2.43·10 ⁹	1.20·10 ⁹	1.40·10 ⁹	1.08·10 ¹⁰	1.12·10 ⁹
Middle East & North Africa	7.07·10 ¹⁰	1.36·10 ⁸	7.07·10 ¹⁰	2.43·10 ⁹	1.20·10 ⁹	1.40·10 ⁹	8.64·10 ⁹	7.84·10 ⁸
Latin America & Caribbean	7.07·10 ¹⁰	1.36·10 ⁸	7.07·10 ¹⁰	2.43·10 ⁹	1.20·10 ⁹	1.40·10 ⁹	1.08·10 ¹⁰	7.84·10 ⁸
Eastern Europe & Central Asia	6.06·10 ¹⁰	1.36·10 ⁸	6.06·10 ¹⁰	2.43·10 ⁹	1.20·10 ⁹	1.40·10 ⁹	1.08·10 ¹⁰	7.84·10 ⁸
East Asia & Pacific	7.07·10 ¹⁰	1.36·10 ⁸	7.07·10 ¹⁰	2.43·10 ⁹	1.20·10 ⁹	1.40·10 ⁹	1.08·10 ¹⁰	7.84·10 ⁸

* as per Weaver et al., (2005) and Wilcock et al., (2006)

180

S1.5 Irrigation

$$L_{irr,p,n} = RF_{irr,n} \cdot C_{irr,p,n}$$

185

[S6]

The only pollutant considered from the irrigation sector in DynQual is TDS. To calculate TDS from the irrigation sector, the return flows from the irrigation sector ($RF_{irr,n}$ in m³ day⁻¹) in gridcell n is multiplied by a mean irrigation drainage concentration ($C_{irr,p,n}$) for pollutant p , which for TDS is in mg l⁻¹ [S6]. As irrigation runoff is rarely collected or treated (Wwap, 2017), no abatement due to wastewater management practices occurs.

190

Irrigation return flows are simulated by PCR-GLOBWB2, under the assumption that withdrawn water that is not consumed (via plant transpiration and open water or soil evaporation) is lost via percolation and contributes to groundwater recharge (Sutanudjaja et al., 2018). Mean irrigation drainage concentrations are derived from the electrical conductivity (dS m⁻¹) averaged over the topsoil (0-30cm) and subsoil (30-100cm) at 0.5° resolution from the ISRIC-WISE global soil database (Batjes, 2005), as per previous work (Van Vliet et al., 2021). Electrical conductivity (EC) is converted to TDS using a TDS/EC ratio for freshwater of 0.7 (Walton, 1989). Mean irrigation drainage concentration is assumed to be constant throughout the study period.

195

200

S1.6 Thermoelectric power

The only pollutant considered from the thermoelectric power sector is water temperature (T_w). Thermal pollution (heat dumps) from the power sector [S7] is calculated based on a spatially-explicit powerplant database containing 13,506 powerplants with detailed information on fuel type and cooling type, representing an estimated 87% of the global thermoelectric capacity in 2015 (Lohrmann et al., 2019).

205

$$L_{pow,Tw,n} = \rho_w \cdot C_p \cdot RF_{pow,n} \cdot \Delta T_{pow_rf} \quad [S7]$$

Where $L_{pow,Tw,n}$ is the heat dump from thermo-electric powerplants (W) in gridcell n , C_p is the specific heat capacity of water ($4,190 \text{ J kg}^{-1} \text{ K}^{-1}$), ρ_w is the density of fresh water (1000 kg m^{-3}), $RF_{pow,n}$ is the return flows of cooling water ($\text{m}^3 \text{ s}^{-1}$) in gridcell n and ΔT_{pow_rf} is the difference in water temperature between the return flows and ambient river water (K).

Water withdrawals and consumption per powerplant are from a spatially explicit powerplant dataset (Lohrmann et al., 2019). These estimates are quantified as a function of plant capacity, load hours and water use intensity, which depends primarily on fuel type and cooling system. The dataset considers five types of cooling systems (wet cooling towers, dry cooling systems, inlet cooling systems, once through cooling and recirculating cooling-pond systems) and four fuel types (nuclear, coal, gas and oil). Power return flows (RF_{pow}) are subsequently calculated by subtracting water consumption from the water withdrawal. We aggregated these power return flows at the gridcell level (5 arc-min) and delineate them in time based upon the construction year of the powerplant. The construction year is derived by cross-referencing powerplant coordinates with information from various other sources (<http://GlobalEnergyObservatory.org/>; <https://datasets.wri.org/dataset/globalpowerplantdatabase>).

A range of values for ΔT_{pow_rf} were found in the literature, varying from between 3 K based upon maximum permissible limits for powerplants in the US as per the Clean Water Act (Van Vliet et al., 2012) to 10 K from once-through systems in the USA in summer months between 2001-2005 (Madden et al., 2013). We selected an intermediate value of 7 K for ΔT_{pow_rf} , as this falls within the range of reported values in the literature and matches well with more recent global thermal emission rates of $\sim 480 \text{ GW}$ (Raptis et al., 2016). Results of a sensitivity analysis also suggests that values for ΔT_{pow_rf} of between 3 – 7 K have relatively moderate impacts on simulated water temperature in thermally polluted basins (Van Vliet et al., 2012).

S1.7 Combined sectoral pollutant loadings

Sectoral loadings of each water quality constituent per gridcell n are converted into consistent units (MW for Tw; g day^{-1} for TDS and BOD; $10^6 \text{ cfu day}^{-1}$ for FC) and aggregated across the contributing sectors, with $L_{TDS,n}$, $L_{BOD,n}$, $L_{FC,n}$ and $L_{Tw,n}$ representing the combined local TDS, BOD, FC and Tw loads in gridcell n [S8].

$$L_{TDS,n} = L_{dom,TDS,n} + L_{man,TDS,n} + L_{usr,TDS,n} + L_{irr,TDS,n}$$

$$L_{BOD,n} = L_{dom,BOD,n} + L_{man,BOD,n} + L_{usr,BOD,n} + L_{intLiv,BOD,n} + L_{extLiv,BOD,n}$$

$$L_{FC,n} = L_{dom,FC,n} + L_{man,FC,n} + L_{usr,FC,n} + L_{intLiv,FC,n} + L_{extLiv,FC,n}$$

$$L_{Tw,n} = L_{pow,Tw,n}$$

[S8]

250 **S2. Implementation of water quality equations**

DynQual uses a numerical scheme (time-explicit fine differences) to simulate the routing of both water and pollutants through the surface water network (based on a local drain direction map), including in-stream processes, with a sub-daily timestep.

255 The length of the time interval (Δt_n in seconds) is estimated with respect to both channel storage and discharge [S9]. This ensures that the length of the time interval is small enough to ensure that flow from gridcell n only flows into the immediately downstream gridcell $n+1$, and not further (i.e. $\Delta t_n > T_n$, where T_n represents the residence time of gridcell n).

$$\Delta t_n = \frac{h_n \cdot A_n \cdot \left(\frac{w_n \cdot l_n}{A_n} \right)}{Q_n}$$

[S9]

260 Where h_n is the water height (m), A_n is the gridcell area (m²), w_n is the channel width (m), l_n is the channel length (m) and Q_n is the discharge (m³ s⁻¹) simulated at the sub-daily timestep using the simplified kinematic wave routing, all in gridcell n .

265 While Δt_n is initially determined per individual gridcell, the shortest calculated interval is used consistently for all gridcells within the simulation extent (Δt). We also set a maximum time-interval (Δt) of 720s (i.e. to ensure that the routing procedure happens at least once every 12 minutes). While we could further increase the numerical accuracy of our simulations by introducing shorter time intervals, this also increases computational times, and thus a balance must be struck (Loucks and Beek, 2017). More information on the implementation of water quality equations within DynQual is available in the open-access model code (<https://github.com/UU-Hydro/DYNQUAL>).

270

S3. Model validation

S3.1 Water quality observations

275 Tw and BOD data was downloaded from the Global River Water Quality Archive (GRQA) (Virro et
 al., 2021), which aggregates data from a variety of datasets including GEMStat (Global Freshwater
 Quality Database) (UNEP, 2020), GLORICH (GLObal River CHEmistry) (Hartmann et al., 2014) and
 WQP (Water Quality Portal) (Read et al., 2017). Electrical conductivity (EC) data was obtained from a
 280 global surface water database (Thorslund and Van Vliet, 2020), which we additionally supplemented
 with GEMStat data (UNEP, 2020), and converted to TDS using a conversion factor of 0.7 (Walton,
 1989). FC data was obtained from GEMStat (UNEP, 2020), additionally supplemented with data from
 the National Water Information System (NWIS) from the United States Geological Survey (USGS)
 (U.S. Geological Survey, 2016). The total number of water quality modelling stations and associated
 observations collated for DynQual validation is presented in Table S8. The number of stations with >30
 285 and >90 measurements across the time period 1980 – 2019 and the associated number of observations
 are also presented (Table S8).

Table S8. Number of water quality monitoring stations and measurements used for DynQual model validation.

Water quality constituent	All stations		Stations > 30 observations		Stations > 90 observations	
	N Stations	N Observations	N Stations	N Observations	N Stations	N Observations
Water Temperature (Tw)	22,990	841,781	7,312	729,813	2,194	474,567
Total Dissolved Solids (TDS)	31,509	6,809,700	26,615	6,722,775	10,494	5,921,049
Biological Oxygen Demand (BOD)	12,604	312,019	2,735	233,169	636	133,106
Fecal Coliform (FC)	7,917	246,652	2,263	213,705	863	136,961

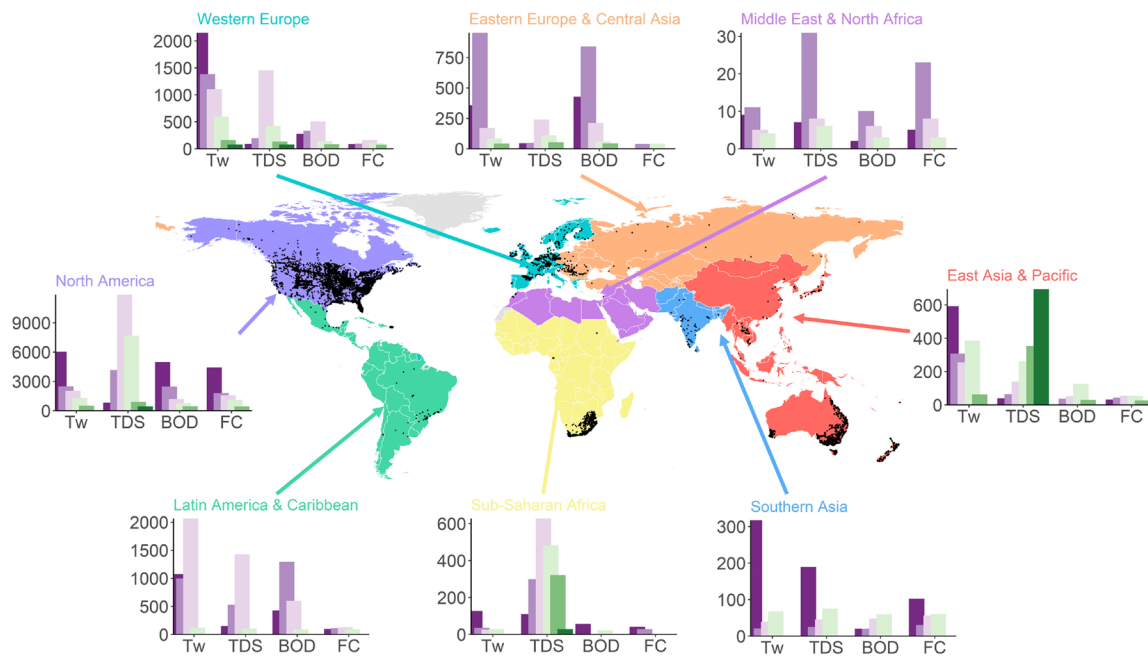
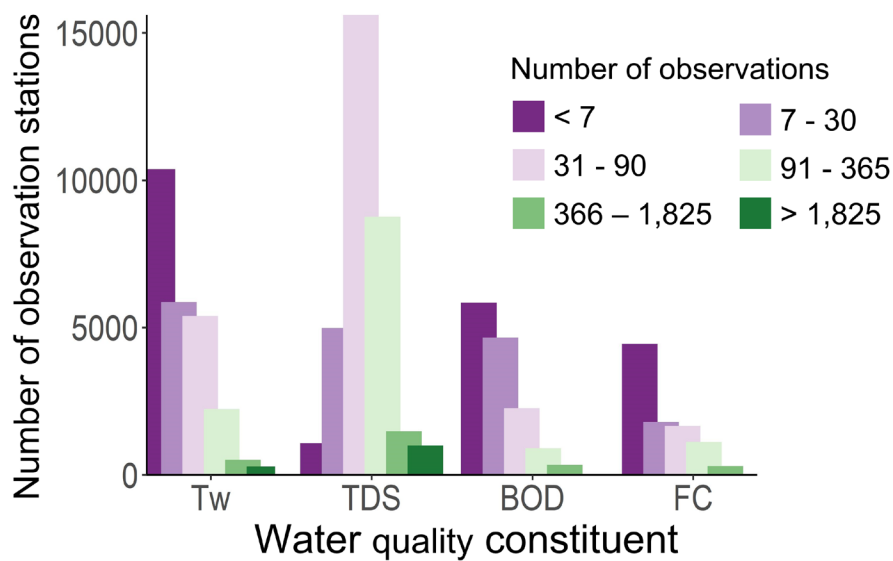
290

295

300 Both the number of water quality monitoring stations and the length of the observation record are highly
unequally distributed across space (Figure S2). Spatial patterns are relatively consistent across all four
water quality constituents. North America is by far the most data-rich world region, with 45%, 76%,
62% and 92% of all monitoring stations for Tw, TDS, BOD and FC located in this region, respectively,
305 accounting for 39%, 32%, 50% and 83% of the total number of observations, respectively. Observations
made across Western Europe account for 28%, 14% and 4% of Tw, BOD and FC of the total data
availability, respectively, but just 3% of the TDS observations. Conversely, 58% of total TDS
observations are from the East Asia & Pacific region, but just 14%, 7% and 3% of the Tw, BOD and
FC observations, respectively. However strong spatial biases within individual regions must also be
310 considered, particularly for TDS observations in East Asia & Pacific where >99% of these observations
are from Australia. The Latin America and Caribbean region also accounts for a small but significant
share of total Tw, TDS, BOD and FC observations, at 13%, 1%, 15% and 3% of total observations,
respectively.

315 Data is extremely scarce across other world regions, especially when also considering the length of
observation records (Figure S2). While there are some localised pockets of high data availability in
different regions (e.g. TDS measurements in South Africa), publicly accessible observational data
records are mostly non-existent. For example, the number of stations in Sub-Saharan Africa with >30
observations of Tw, BOD and FC is just 10, 1 and 1, respectively. When considering stations with >90
320 observations, these numbers drop to 6, 1 and 0. Similar patterns in data availability are observed for the
Middle East and North Africa and Southern Asia regions.

The spatial biases in the observed data, combined with data availability issues in general (especially for
BOD and FC), provide acute challenges for the evaluation of global water quality models across
325 different world regions (Section SI 3.2).



330 **Figure S2.** Number of surface water quality monitoring stations per world region, disaggregated by the total number of observations made at each site from 1980 - 2019. Black dots on the map display the locations of water quality monitoring stations with > 90 observations of any water quality constituent. Please note that different numbers are used on the vertical axis for bar charts displaying the number of observation stations for different world regions.

335

S3.2 Model evaluation

340 S3.2.1 Concentration classes

As per Jones et al., (2022), we evaluate model performance for TDS, BOD and FC with respect to pollutant classes linked to key sectoral water quality thresholds (Table S9), which are derived from extensive literature research (UNEP, 2016). TDS thresholds are based upon irrigation water quality standards (Fipps, 2003; Zaman et al., 2018), with < 525 mg l⁻¹ designated as “good”, 525 – 2,100 mg l⁻¹ as “permissible to doubtful” and > 2,100 mg l⁻¹ as “unsuitable”. BOD thresholds are linked to environmental standards, with < 4 mg l⁻¹ designating low pollution (“sufficient oxygen and high species diversity”), 4 – 8 mg l⁻¹ designating moderate pollution (“suspended discharges occur but have no major effect on biota”) and > 8 mg l⁻¹ designating high pollution (“depletion of oxygen can result in fish kills”) (UNEP, 2016). FC thresholds are based upon human health concerns related to direct contact, with high pollution designated as >1,000 cfu 100ml⁻¹ (“unsuitable for direct human contact”), and < 200 cfu 100ml⁻¹ representing no risk to human health (UNEP, 2016).

355 **Table S9.** Total dissolved solids (TDS), biological oxygen demand (BOD) and fecal coliform (FC) concentration thresholds denoting the pollution status of a freshwater body as “low”, “moderate” or “high”.

Pollutant Status	TDS (mg l ⁻¹)	BOD (mg l ⁻¹)	FC (cfu 100ml ⁻¹)
Low	< 525	< 4	< 200
Moderate	525 – 2,100	4 – 8	200 – 1,000
High	> 2,100	> 8	> 1,000

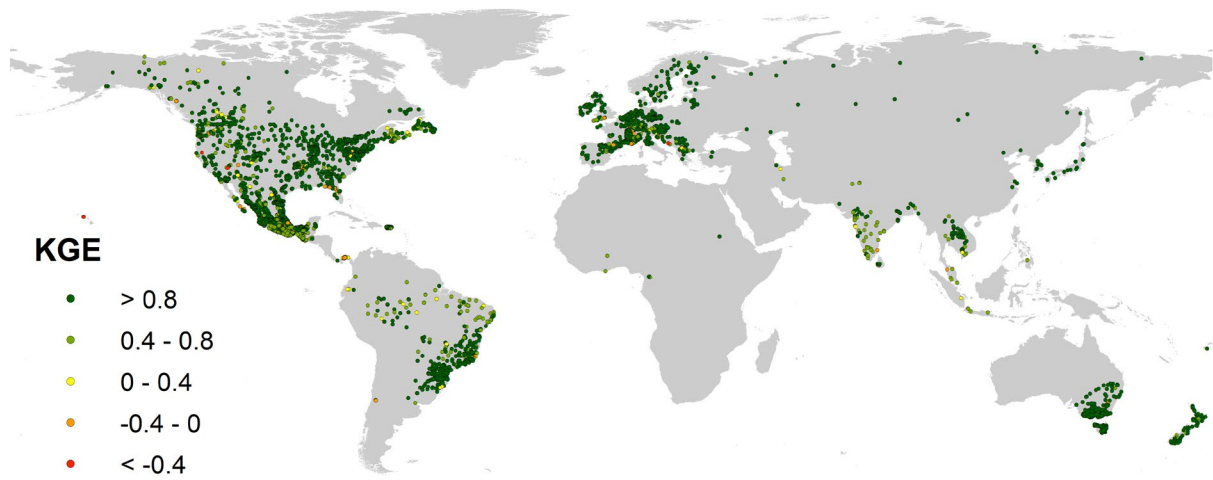
360 S3.2.2 Statistical evaluation metrics

For Tw, model performance is evaluated statistically using the Kling-Gupta efficiency (KGE) coefficient [S10] (Gupta et al., 2009).

$$365 \quad KGE = 1 - \sqrt{(r - 1)^2 + (\alpha - 1)^2 + (\beta - 1)^2} \quad [S10]$$

Where r is the linear correlation between observations and simulations, α is a measure of the flow variability error, and β a bias term. KGE values of 1 indicate perfect agreement between observations and simulations, while KGE values exceeding -0.4 indicate that a model improved upon a mean benchmark (Knoben et al., 2019).

370 Spatial patterns in KGE for water temperature simulations by DynQual are displayed in Figure S3 and are described in the manuscript.



375

Figure S3. Spatial validation of water temperature (T_w) observations versus simulations using the Kling-Gupta efficiency (KGE) at for observation stations with > 30 observations over 1980 – 2019.

380

For TDS, BOD and FC, model performance is evaluated statistically using the root mean square error normalised by the mean (nRMSE) [S11]

$$nRMSE = \frac{\sqrt{\frac{\sum_{i=1}^N (Sim_i - Obs_i)^2}{n}}}{\bar{Obs}}$$

[S11]

385

Patterns in nRMSE for TDS, BOD and FC simulations are displayed in Figure S4a-c and are described in the manuscript.

390

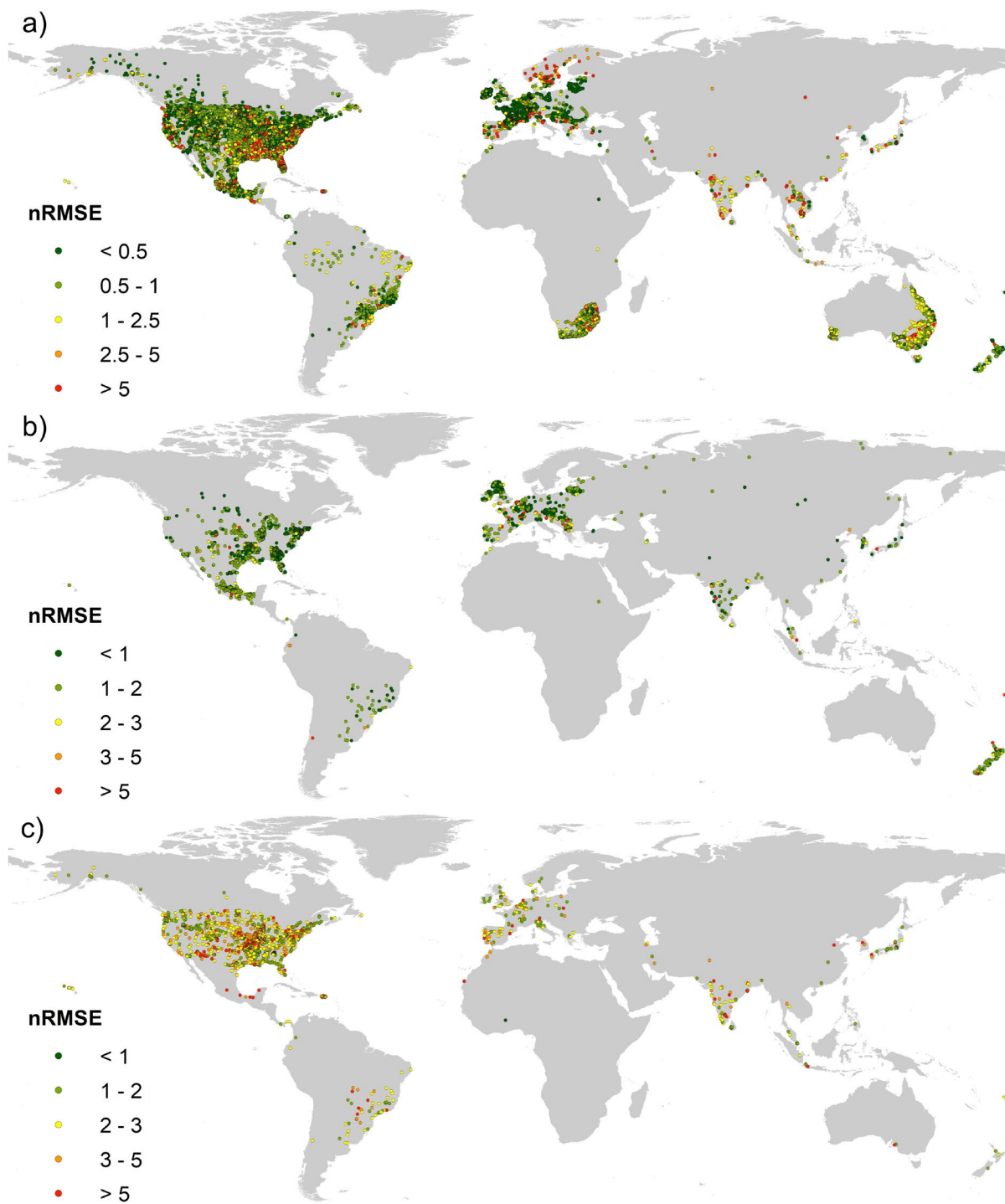
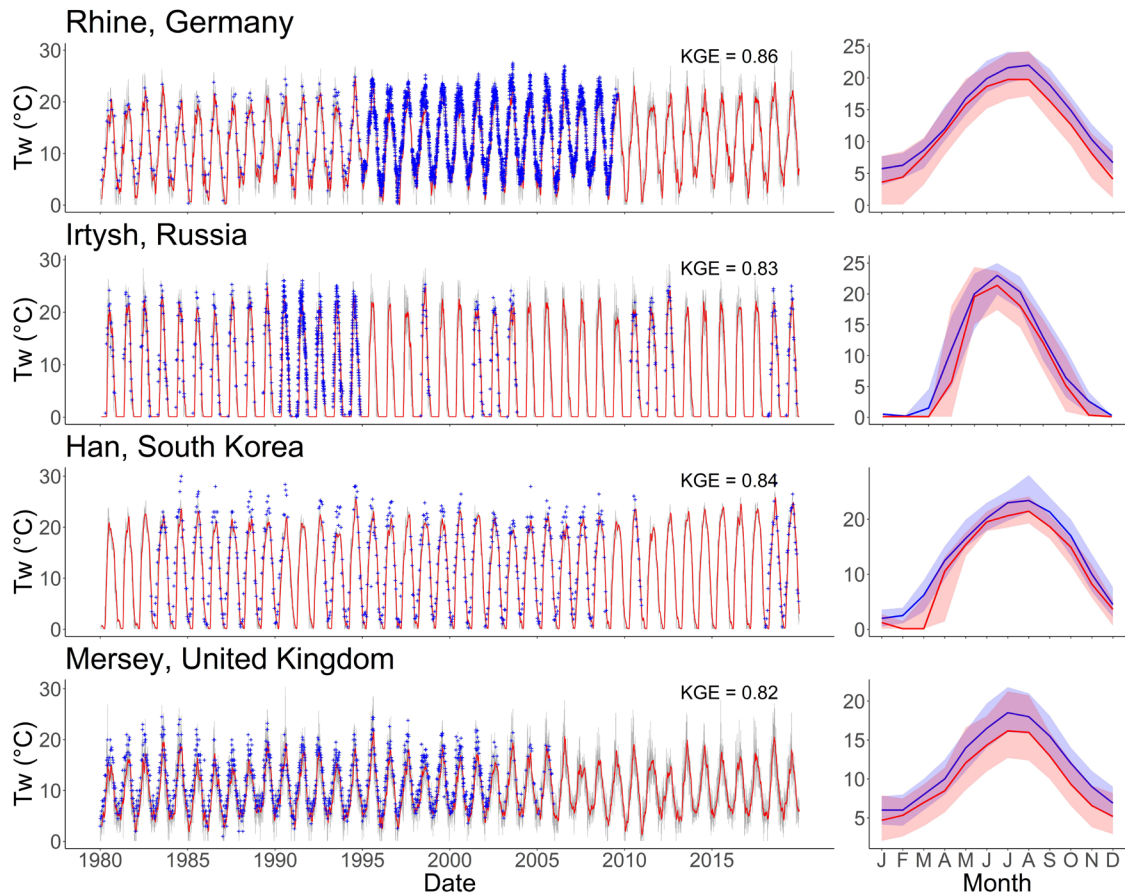


Figure S4. Spatial validation of a) total dissolved solids (TDS); b) biological oxygen demand; and c) fecal coliform (FC) observations versus simulations using the normalised root mean square error (nRMSE) at for observation stations with > 30 observations over 1980 – 2019.

395

S3.2.3 Time-series and average annual cycles

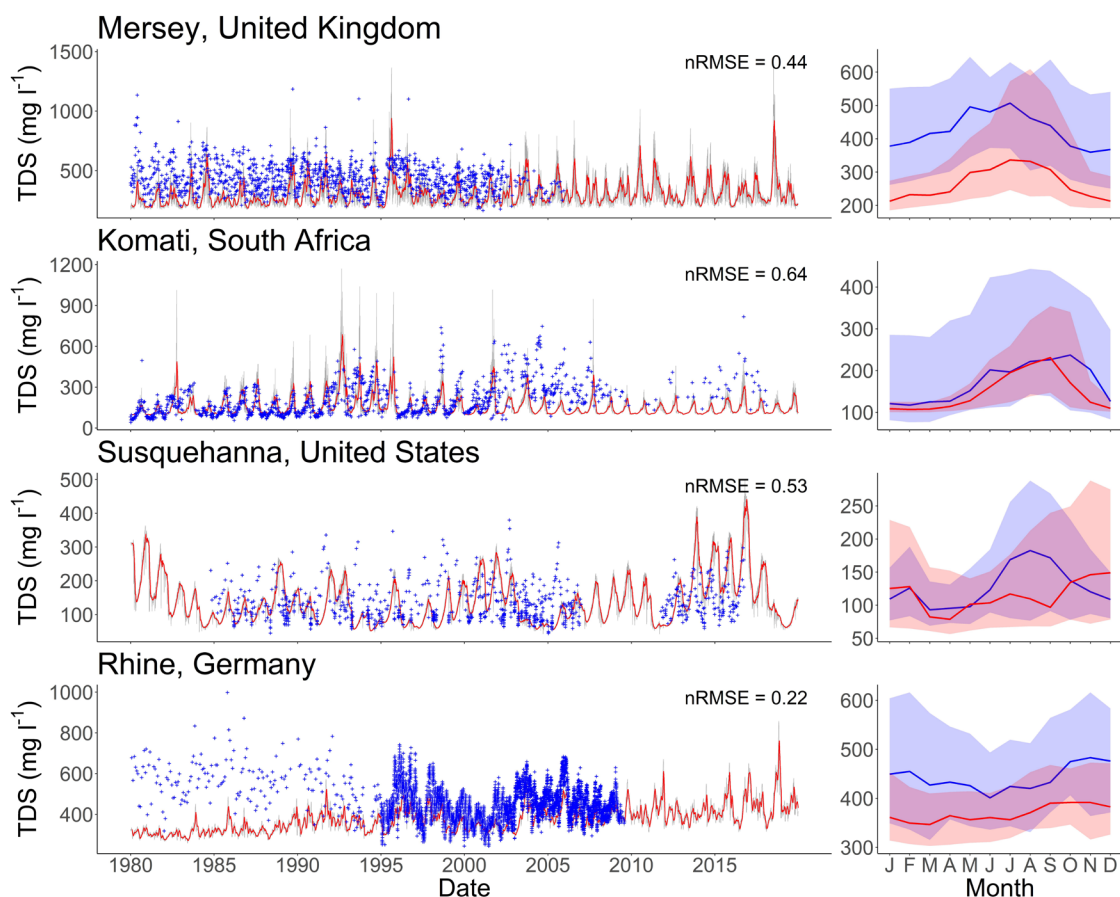
400 Supplementing the time-series and average annual cycles displayed in the manuscript (Figure 5), results from additional stations are presented for Tw (Figure S5), TDS (Figure S6), BOD (Figure S7) and FC (Figure S8).



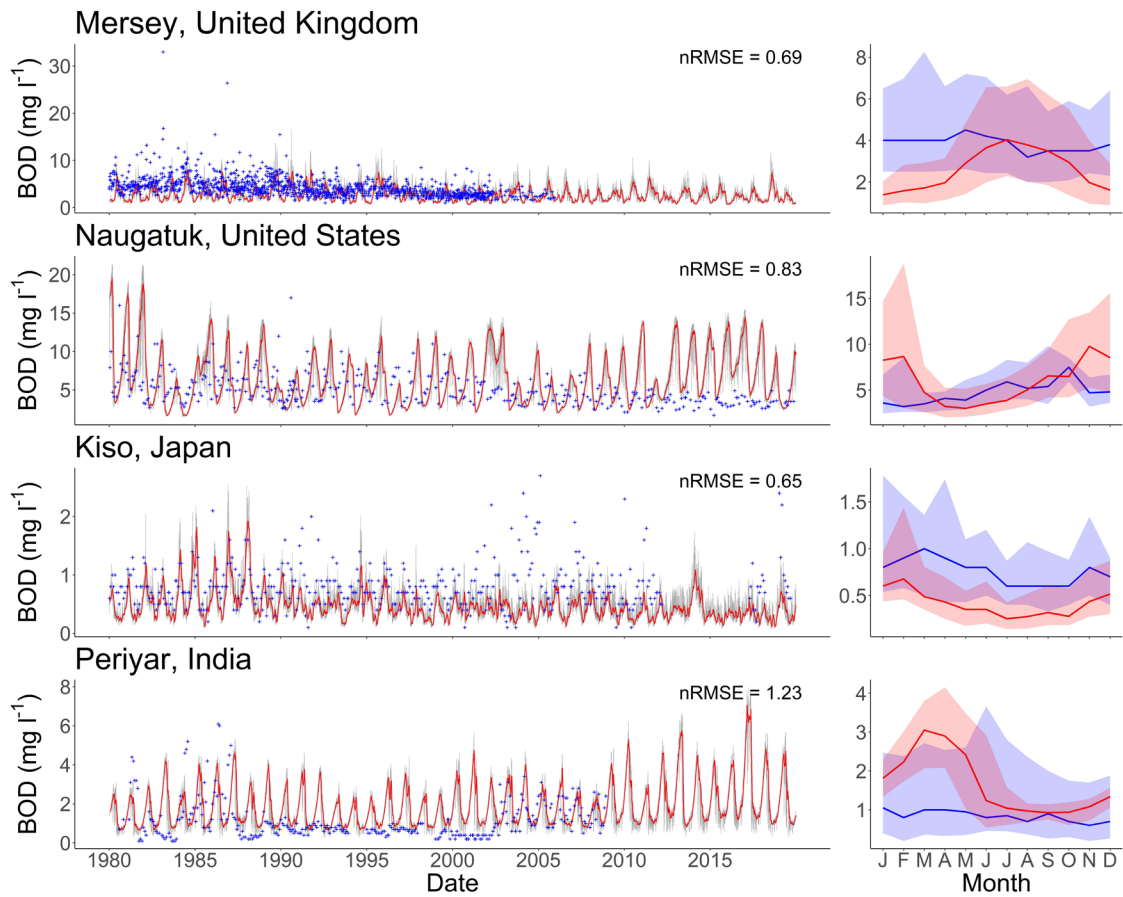
405

Figure S5. Time-series (left) and average annual cycles (right) of observed versus simulated water temperature (°C) at four selected monitoring stations. In the time-series plots, observations are indicated by blue crosses, daily simulations by grey lines and 30 day running averages by red lines. In the average annual cycles plots, blue and red lines indicated the median observed and simulated water temperature, respectively, while the shading represents the range in water temperatures as indicated by the 10th and 90th percentiles.

410



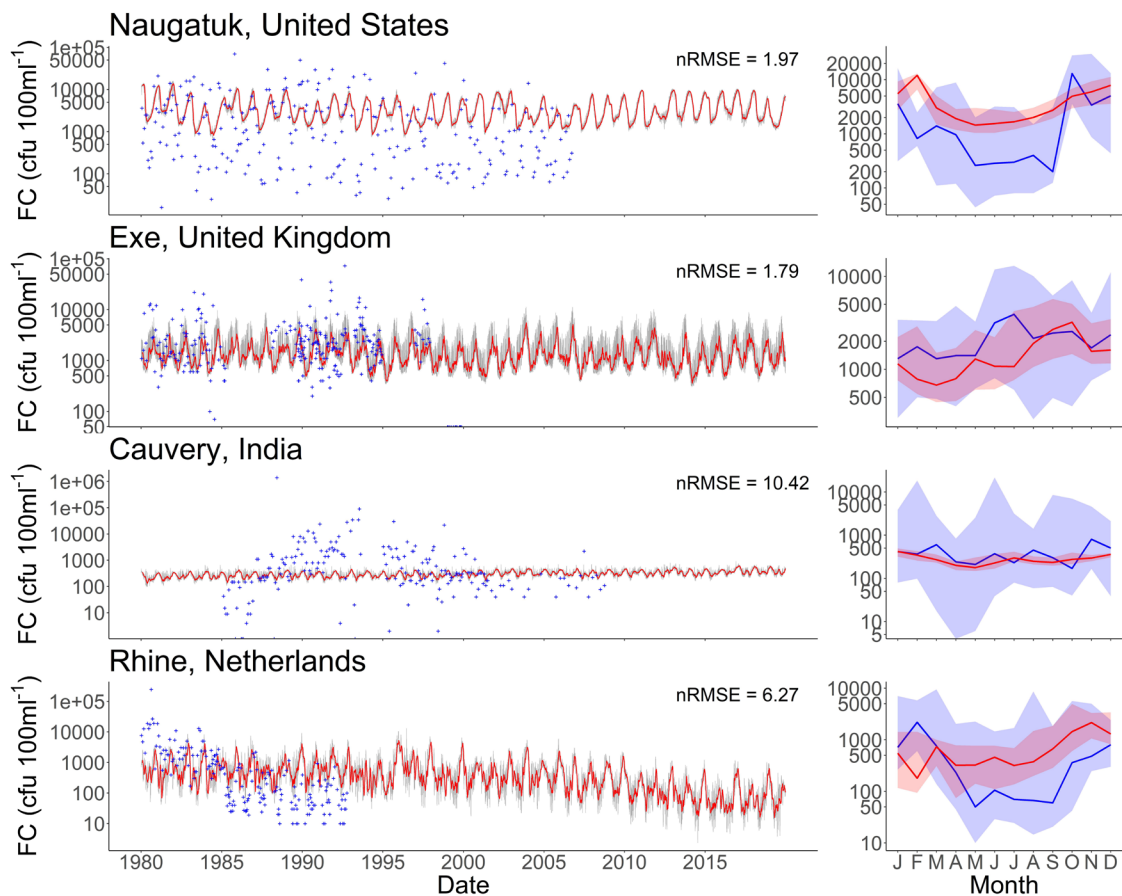
415 **Figure S6.** Time-series (left) and average annual cycles (right) of observed versus simulated total dissolved solids (TDS) concentrations (mg l⁻¹) at four selected monitoring stations. In the time-series plots, observations are indicated by blue crosses, daily simulations by grey lines and 30 day running averages by red lines. In the average annual cycles plots, blue and red lines indicated the median observed and simulated concentrations, respectively, while the shading represents the range in concentrations as indicated by the 10th and 90th percentiles.



420

425

Figure S7. Time-series (left) and average annual cycles (right) of observed versus simulated biological oxygen demand (BOD) concentrations (mg l^{-1}) at four selected monitoring stations. In the time-series plots, observations are indicated by blue crosses, daily simulations by grey lines and 30 day running averages by red lines. In the average annual cycles plots, blue and red lines indicated the median observed and simulated concentrations, respectively, while the shading represents the range in concentrations as indicated by the 10th and 90th percentiles.



430 **Figure S8.** Time-series (left) and average annual cycles (right) of observed versus simulated fecal coliform (FC) concentrations ($\text{cfu } 100\text{ml}^{-1}$) at four selected monitoring stations. In the time-series plots, observations are indicated by blue crosses, daily simulations by grey lines and 30 day running averages by red lines. In the average annual cycles plots, blue and red lines indicated the median observed and simulated concentrations, respectively, while the shading represents the range in concentrations as indicated by the 10th and 90th percentiles.

435

S3.3 Examples of issues in observational records

440 To evaluate the performance of DynQual, data from ~57,000 individual water quality monitoring
stations was collated from various data sources (SI Section 3.1). While this is beneficial for having a
greater number of observations, this procedure also introduces additional challenges for model
evaluation. We illustrate some examples of issues within the observational records themselves in
Figure S9, including a) artefacts in data records; b) issues related to detection limits or reporting
accuracies; and c) large variability in the observational records.

445

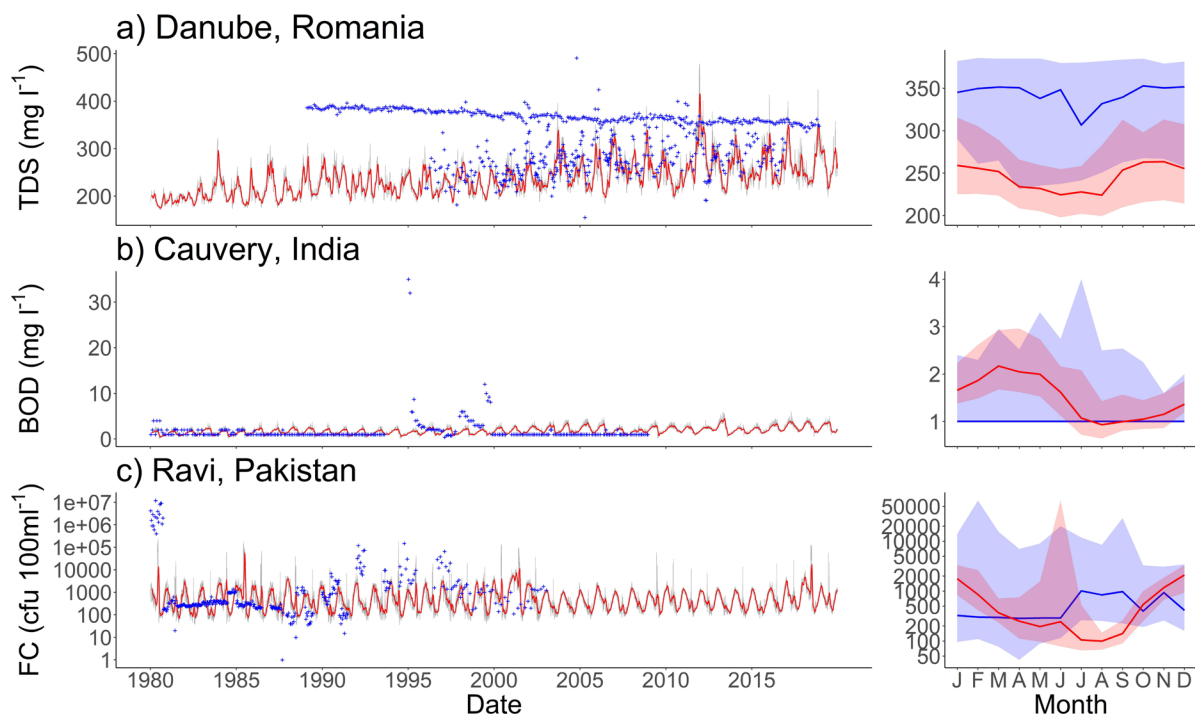


Figure S9. Examples of challenges associated with observation data when evaluating global surface water quality models: a) artefacts in the data; b) detection limits or reporting accuracy; c) large variability in the observed record.

450

References

- 455 Batjes, N. H.: ISRIC-WISE global data set of derived soil properties on a 0.5 by 0.5 degree grid (Version 3.0). World Soil Information, Wageningen, 24, 2005.
- Fipps, G.: Irrigation water quality standards and salinity management strategies, Texas FARMER Collection, 2003.
- 460 Gilbert, M., Nicolas, G., Cinardi, G., Van Boeckel, T. P., Vanwambeke, S. O., Wint, G. R. W., and Robinson, T. P.: Global distribution data for cattle, buffaloes, horses, sheep, goats, pigs, chickens and ducks in 2010, *Scientific Data*, 5, 180227, [10.1038/sdata.2018.227](https://doi.org/10.1038/sdata.2018.227), 2018.
- Gupta, H. V., Kling, H., Yilmaz, K. K., and Martinez, G. F.: Decomposition of the mean squared error and NSE performance criteria: Implications for improving hydrological modelling, *Journal of Hydrology*, 377, 80-91, <https://doi.org/10.1016/j.jhydrol.2009.08.003>, 2009.
- 465 Hartmann, J., Lauerwald, R., and Moosdorf, N.: A Brief Overview of the GLObal RIVER Chemistry Database, *GLORICH, Procedia Earth and Planetary Science*, 10, 23-27, <https://doi.org/10.1016/j.proeps.2014.08.005>, 2014.
- Jones, E. R., van Vliet, M. T. H., Qadir, M., and Bierkens, M. F. P.: Country-level and gridded estimates of wastewater production, collection, treatment and reuse, *Earth Syst. Sci. Data*, 13, 237-254, [10.5194/essd-13-237-2021](https://doi.org/10.5194/essd-13-237-2021), 2021.
- 470 Jones, E. R., Bierkens, M. F. P., Wanders, N., Sutanudjaja, E. H., van Beek, L. P. H., and van Vliet, M. T. H.: Current wastewater treatment targets are insufficient to protect surface water quality, *Communications Earth & Environment*, 3, 221, [10.1038/s43247-022-00554-y](https://doi.org/10.1038/s43247-022-00554-y), 2022.
- 475 Knoben, W. J. M., Freer, J. E., and Woods, R. A.: Technical note: Inherent benchmark or not? Comparing Nash–Sutcliffe and Kling–Gupta efficiency scores, *Hydrol. Earth Syst. Sci.*, 23, 4323-4331, [10.5194/hess-23-4323-2019](https://doi.org/10.5194/hess-23-4323-2019), 2019.
- Lange, S. and Geiger, T.: ISIMIP3a population input data (1.0) [dataset], [10.48364/ISIMIP.822480](https://doi.org/10.48364/ISIMIP.822480), 2020.
- 480 Lohrmann, A., Farfan, J., Caldera, U., Lohrmann, C., and Breyer, C.: Global scenarios for significant water use reduction in thermal power plants based on cooling water demand estimation using satellite imagery, *Nature Energy*, 4, 1040-1048, [10.1038/s41560-019-0501-4](https://doi.org/10.1038/s41560-019-0501-4), 2019.
- Loucks, D. P. and Beek, E. v.: Water quality modeling and prediction, in: *Water resource systems planning and management*, Springer, 417-467, 2017.
- 485 Madden, N., Lewis, A., and Davis, M.: Thermal effluent from the power sector: an analysis of once-through cooling system impacts on surface water temperature, *Environmental Research Letters*, 8, 035006, [10.1088/1748-9326/8/3/035006](https://doi.org/10.1088/1748-9326/8/3/035006), 2013.
- Raptis, C. E., van Vliet, M. T. H., and Pfister, S.: Global thermal pollution of rivers from thermoelectric power plants, *Environmental Research Letters*, 11, 104011, [10.1088/1748-9326/11/10/104011](https://doi.org/10.1088/1748-9326/11/10/104011), 2016.
- 490 Read, E. K., Carr, L., De Cicco, L., Dugan, H. A., Hanson, P. C., Hart, J. A., Kreft, J., Read, J. S., and Winslow, L. A.: Water quality data for national-scale aquatic research: The Water Quality Portal, *Water Resources Research*, 53, 1735-1745, <https://doi.org/10.1002/2016WR019993>, 2017.
- Robinson, T. P., Thornton, P. K., Franceschini, G., Kruska, R., Chiozza, F., Notenbaert, A. M. O., Cecchi, G., Herrero, M. T., Epprecht, M., and Fritz, S.: Global livestock production systems, *Food and*

Agriculture Organization of the United Nations (FAO) and International Livestock Research Institute (ILRI), Rome, 152 pp pp.2011.

495 Sutanudjaja, E., Beek, R., Wanders, N., Wada, Y., Bosmans, J., Drost, N., Ent, R., de Graaf, I., Hoch, J., de Jong, K., Karssenber, D., López, P., Pessenteiner, S., Schmitz, O., Straatsma, M., Vannamettee, E., Wisser, D., and Bierkens, M.: PCR-GLOBWB 2: A 5 arcmin global hydrological and water resources model, *Geoscientific Model Development*, 11, 2429-2453, 10.5194/gmd-11-2429-2018, 2018.

500 Thomson, K.: *World agriculture: towards 2015/2030: an FAO perspective*: Jelle Briunsmma (Ed.), FAO/Earthscan, 2003. 432 pp. ISBNs: 92 5 104835 5 (FAO paperback), 1 84407 007 7 (Earthscan paperback) and 1 84407 008 57 (Earthscan hardback), *Land Use Policy*, 20, 375, 10.1016/S0264-8377(03)00047-4, 2003.

505 Thorslund, J. and van Vliet, M. T. H.: A global dataset of surface water and groundwater salinity measurements from 1980–2019, *Scientific Data*, 7, 231, 10.1038/s41597-020-0562-z, 2020.

U.S. Geological Survey: National Water Information System data available on the World Wide Web (USGS Water Data for the Nation) [dataset], <http://dx.doi.org/10.5066/F7P55KJN>, 2016.

UNEP: *A Snapshot of the World's Water Quality: Towards a global assessment*, United Nations Environment Programme, Nairobi, Kenya, 162pp, 2016.

510 UNEP: GEMStat database of the Global Environment Monitoring System for Freshwater (GEMS/Water) Programme., 2020.

van Vliet, M., Yearsley, J., Ludwig, F., Vögele, S., Lettenmaier, D., and Kabat, P.: Vulnerability of US and European Electricity Supply to Climate Change, *Nature Climate Change*, 2, 676-681, 10.1038/nclimate1546, 2012.

515 van Vliet, M. T. H., Jones, E. R., Flörke, M., Franssen, W. H. P., Hanasaki, N., Wada, Y., and Yearsley, J. R.: Global water scarcity including surface water quality and expansions of clean water technologies, *Environmental Research Letters*, 16, 024020, 10.1088/1748-9326/abbfc3, 2021.

520 Vigiak, O., Grizzetti, B., Udias-Moinelo, A., Zanni, M., Dorati, C., Bouraoui, F., and Pistocchi, A.: Predicting biochemical oxygen demand in European freshwater bodies, *Science of The Total Environment*, 666, 1089-1105, <https://doi.org/10.1016/j.scitotenv.2019.02.252>, 2019.

Virro, H., Amatulli, G., Kmoch, A., Shen, L., and Uemaa, E.: GRQA: Global River Water Quality Archive, *Earth Syst. Sci. Data*, 13, 5483-5507, 10.5194/essd-13-5483-2021, 2021.

Walton, N. R. G.: Electrical Conductivity and Total Dissolved Solids—What is Their Precise Relationship?, *Desalination*, 72, 275-292, [https://doi.org/10.1016/0011-9164\(89\)80012-8](https://doi.org/10.1016/0011-9164(89)80012-8), 1989.

525 Wen, Y., Schoups, G., and van de Giesen, N.: Organic pollution of rivers: Combined threats of urbanization, livestock farming and global climate change, *Scientific Reports*, 7, 43289, 10.1038/srep43289, 2017.

530 Williams, R., Keller, V., Voß, A., Bärlund, I., Malve, O., Riihimäki, J., Tattari, S., and Alcamo, J.: Assessment of current water pollution loads in Europe: estimation of gridded loads for use in global water quality models, *Hydrological Processes*, 26, 2395-2410, <https://doi.org/10.1002/hyp.9427>, 2012.

WWAP: *The United Nations World Water Development Report 2017. Wastewater: The Untapped Resource*, Paris, UNESCO, 2017.

535 Zaman, M., Shahid, S. A., and Heng, L.: Irrigation Water Quality, in: Guideline for Salinity Assessment, Mitigation and Adaptation Using Nuclear and Related Techniques, Springer International Publishing, Cham, 113-131, 10.1007/978-3-319-96190-3_5, 2018.